Non-rigid registration of point clouds using landmarks and stochastic neighbor embedding

Amar Maharjan,[a] Xiaohui Yuan,[a,*] Qiang Lu,[b] Yuqi Fan,[b] and Tian Chen[b]

[a]University of North Texas, Department of Computer Science and Engineering, Denton, Texas, United States

[b]Hefei University of Technology, Hefei, China

Abstract. Our study presents a probabilistic non-rigid point set registration method to deal with large and uneven deformations. Our method treats the registration as a density estimation problem. In our method, we add two key constraints to enforce landmark correspondences and preserve local neighborhood structure. We assume that the landmarks, which represent the salient points in the point sets, are given or can be detected using keypoint detectors such as scale-invariant feature transform or MeshDOG. By enforcing landmark correspondences, we preserve the overall global shape of the point set with significant deformations. Furthermore, by leveraging stochastic neighbor embedding, we incorporate constraints to preserve local neighborhood structure, which penalizes incoherent transformation within a neighborhood. Our experimental results in both 2D and 3D datasets show that our method outperforms state-of-the-art methods in a large degree of deformations. In particular, quantitative results show that the error is 29% better than the second-best result (from the state-of-the-art methods). Our analysis shows that a relatively small number of landmarks is sufficient to deal with large deformations. Finally, our study shows that our method is computationally comparable to state-of-the-art methods. © *2021 SPIE and IS&T* [DOI: 10.1117/1.JEI.30.3.031202]

Keywords: non-rigid registration; landmark; deformation; local neighborhood structure.

Paper 200550SS received Aug. 11, 2020; accepted for publication Oct. 20, 2020; published online Jan. 5, 2021.

1 Introduction

Registration of point set identifies correspondences between two sets of points, from which a transformation function is derived to achieve alignment. It is a fundamental task in many computer vision and pattern recognition applications such as range image-based human pose tracking, three-dimensional object reconstruction,[1] transfer of information,[2,3] and medical image registration.[4] In such applications, however, large deformations make point set registration a challenging task.[5]

To address non-rigid deformation, coherent point drift (CPD) was proposed to regulate the transformations of points within a neighborhood.[6] This method assumes that the transformation for points that are in close vicinity is highly similar. Ge et al.[7] and Ge and Fan[8] extended the CPD method by adding constraints to handle non-rigid and articulated deformations. In their method, the authors added local linear embedding (LLE)[9] and the Laplacian coordinate (LC) to maintain local neighborhood structure and scale, respectively. Several other methods have introduced techniques to preserve the local neighborhood structure of point set.[10–12] Ma et al.[11] used feature descriptors such as shape context[13] and fast point feature histogram[14] to ensure the local structure of point subsets. Despite the success demonstrated by the aforementioned methods, obtaining accurate correspondences between point sets and maintaining the shape and structure in the case of large and uneven deformation after transformation is still an open challenge in non-rigid point set registration. In the applications of tracking humans in actions, for example, deformation from movements of limbs is common. As a consequence, the body shape appears dramatically

*Address all correspondence to Xiaohui Yuan, xiaohui.yuan@unt.edu

1017-9909/2021/$28.00 © 2021 SPIE and IS&T

Downloaded From: https://www.spiedigitallibrary.org/journals/Journal-of-Electronic-Imaging on 23 Apr 2021
Terms of Use: https://www.spiedigitallibrary.org/terms-of-use

differently, whereas the local structure of a rigid body part remains unchanged. So, in such large uneven deformations during registration, maintaining local neighborhood structure of point set and avoiding getting trapped on local minima is critical for accurate results.

In this paper, we present a non-rigid point set registration method by incorporating constraints of corresponding landmarks to register point sets that represent a large deformation. Landmarks represent the salient points in point sets and can be identified using methods such as scale-invariant feature transform[15] or MeshDOG.[16] In our evaluation, we manually select landmarks in the point clouds and their correspondences. The correspondence between landmarks enables us to regulate the optimization process. In addition, by leveraging stochastic neighbor embedding (SNE),[17] we aim to penalize incoherent transformation within a neighborhood and hence preserve the local structure.

The remainder of this paper is organized as follows: Section 2 reviews the related methods for non-rigid point set registration. Section 3 presents our proposed method for non-rigid point set registration. Section 4 discusses our experimental results and comparison with state-of-the-art methods. Section 5 concludes this paper with a summary.

2 Related Work

Iterative closest point (ICP) is one of the earliest methods for rigid point set registration.[18,19] The ICP method is very popular due to its simplicity and computational efficiency. The method has two iterative steps: first, compute the closest point correspondences from one point set to another point set, and then obtain the best transformation parameters using the mean least square problem given the correspondences. The method iterates these two steps until convergence. Later, many modifications to the ICP have been proposed,[20] and it has been extended to support non-rigid registration.[21] Chui et al.[22,23] proposed a general framework based on robust point matching.[24] In this framework, the authors used thin-plate spline (TPS) as a non-rigid spatial mapping, which performs a soft assignment, instead of binary assignment, for point correspondence and employs deterministic annealing to favor global rigid transformations at the early stage of the optimization and local, non-rigid transformations in a later stage using thin-plate-splines. Tin et al.[25] proposed kernel correlation by extending the correlation technique to point set registration. This method also used soft correspondence assignment, and the correlation of the two kernel density estimates was the main part of the cost function. A similar strategy was used by Jain et al.,[26] in which the point sets were modeled as Gaussian mixtures, and the registration problem was formulated as minimizing the L2 distance between the two Gaussian mixtures.

One popular method for non-rigid registration is a probabilistic approach in which the registration is mapped into density estimation based on Gaussian mixture model (GMM). In this approach, GMM centroids are represented by one point set (template or model) and the other point set represents the input data. The template points are transformed with prior constraints so that the point sets are aligned as much as possible by maximum likelihood fashion. Several of the earliest methods using this probabilistic technique are in.[27,28] The authors in these methods used GMM to identify hand-printed digits. Initially, individual GMM centroids are equally spaced around the spline and the model is fitted to the image using the expectation–maximization (EM) technique. Chui et al.[29] proposed a general point matching framework using GMM, called mixture point matching, for both rigid and non-rigid (TPS-based) registration under the presence of noise and outliers. CPD is a robust probabilistic point set registration method based on GMM; the key idea is moving points coherently to maintain the topological structure of the point set[6] based on the motion coherence theory.[30] Extensions to the CPD have been proposed to preserve point set structure and the intrinsic geometry of the data.[7,8,11,12,31] Panaganti et al.[12] proposed using proximity weight between the points using shape context[13] to calculate correspondences and a graph-Laplacian regularization term to preserve the intrinsic geometry of the point set. Ge et al.[7] and Ge and Fan[8] extended the CPD method, called local structure preservation (LSP), to handle complex non-rigid and articulated deformations by adding two regularization terms, LLE[9] and LC, to maintain the local neighborhood relationship and scale (size), respectively. Instead of using equal membership probabilities to the mixture model such as that in some

Downloaded From: https://www.spiedigitallibrary.org/journals/Journal-of-Electronic-Imaging on 23 Apr 2021
Terms of Use: https://www.spiedigitallibrary.org/terms-of-use

works,[6,8] recent methods have assigned membership probabilities to the mixture model; they show robustness to noises, outliers, and occlusions.[11,31] The idea is to match similar local neighborhood structures between point sets with the help of feature descriptors.[13,14,32] However, these methods are vulnerable to a local minimum in case of large and uneven deformations. Also the assumption of similar local structure in both point sets is problematic as distortions and stretches are always present in real data.

Another registration strategy is point matching, which contains two steps.[33–36] First, a set of initial correspondences is created using feature descriptors matching, which usually contains a large number of incorrect correspondences, outliers. Second, points are transformed with the constraint to identify the true correspondences and filter out the outliers. Ma et al.[33] proposed a method, called vector field consensus (VFC), that created a set of putative correspondences using a local feature descriptor, such as shape context[13] for 2D and MeshHOG[37] for 3D, and then identified correct correspondences by interpolating a smooth vector field between the point sets. Later, the VFC method was extended with manifold regularization[38] by Refs. 34 and 35, in which the manifold regularization was used to preserve the intrinsic structure of the point set.

Other methods that used constraints to preserve local neighborhood structures or intrinsic geometry of point sets for robust point set registration are in Refs. 10 and 39. Zheng and Doermann[10] proposed a method for a general point matching problem to preserve local neighborhood structures using a graph matching technique. It used shape context[13] for good initialization to avoid local optimum for 2D point sets but was unclear on 3D point sets. Wang et al.[39] presented context-aware Gaussian fields that used inner-distance shape context[32] for initial correspondences between the point sets and added the Laplacian regularized regularization term to preserve the intrinsic geometry of transformed point set. Learning-based registration methods have also been proposed.[40] Wang at el.[41] proposed a learning-based method, called deep closest point, to address the issues of the classical ICP method such as stalling in suboptimal local optima.

3 Method

Our method takes two sets of points as inputs and corresponding landmarks as a strong constraint. The optimization process leverages the GMM that enforces both local coherence using SNE and global constraint through landmarks.

3.1 *Problem Formulation*

Let X and Y denote two sets of points in a D-dimensional space. We have $X = \{\mathbf{x}_1, \mathbf{x}_2, \ldots, \mathbf{x}_N\}$ and $Y = \{\mathbf{y}_1, \mathbf{y}_2, \ldots, \mathbf{y}_M\}$, where M and N denote the number of points of the respective set. Assume noise follows the uniform distribution, i.e., $p_n^* = \frac{1}{N}$; the probability density function of point $\mathbf{x}_n$ given Y is as follows:

$$p(\mathbf{x}_n) = \sum_{m=1}^{M} p(\mathbf{x}_n|\mathbf{y}_m)p(\mathbf{y}_m) + p_n^*, \tag{1}$$

where $p(\mathbf{y}_m) = \frac{1}{M}$. We assume the moving point set $\mathbf{Y}$ as the GMM centroids and the other point set $\mathbf{X}$ as the fixed point set. Further, we also assume equal isotropic covariances $\sigma^2\mathbf{I}$ for all GMM components, where $\mathbf{I}$ is an identity matrix. Let $\gamma \in [0,1]$ denote the rate of noise and outlier in the observed dataset X, and Eq. (1) is rewritten as follows:

$$p(\mathbf{x}_n) = \frac{(1-\gamma)}{M} \sum_{m=1}^{M} \frac{1}{(2\pi\sigma^2)^{D/2}} \exp\left(-\frac{\|\mathbf{x}_n - \mathbf{y}_m\|^2}{2\sigma^2}\right) + \frac{\gamma}{N}. \tag{2}$$

Given that the points in X are independent and identically distributed, the joint probability of X is

Downloaded From: https://www.spiedigitallibrary.org/journals/Journal-of-Electronic-Imaging on 23 Apr 2021
Terms of Use: https://www.spiedigitallibrary.org/terms-of-use

$$p(X) = \prod_{n=1}^{N} p(\mathbf{x}_n). \tag{3}$$

By taking the negative logarithm on both sides of Eq. (3), we have

$$E = -\ln L = -\ln p(X) = -\sum_{n=1}^{N} \ln p(\mathbf{x}_n), \tag{4}$$

which can be regarded as an error function; minimizing E is then equivalent to maximizing the likelihood L.[42] Following the work in Ref. 42, we use the EM algorithm to find the best set of parameters, θ and σ^2, of the mixture model for maximum likelihood. We minimize the following function after dropping terms independent of the parameters:

$$Q(\boldsymbol{\theta}, \sigma^2) = \frac{1}{2\sigma^2} \sum_{n,m=1}^{N,M} p^{i-1}(\mathbf{y}_m|\mathbf{x}_n)\|\mathbf{x}_n - \tau(\mathbf{y}_m)\|^2 + \frac{N_P D}{2} \ln \sigma^2, \tag{5}$$

where

$$p^{(i-1)}(\mathbf{y}_m|\mathbf{x}_n) = \frac{\exp\left[-\frac{1}{2}\left\|\frac{\mathbf{x}_n - \tau(\mathbf{y}_m)}{\sigma_{(i-1)}}\right\|^2\right]}{\sum_{k=1}^{M} \exp\left[-\frac{1}{2}\left\|\frac{\mathbf{x}_n - \tau(\mathbf{y}_k)}{\sigma_{(i-1)}}\right\|^2\right] + C}, \tag{6}$$

and $C = \gamma[2\pi\sigma^2_{(i-1)}]^{D/2}M/[(1-\gamma)N]$, τ is a transformation function that maps a point $\mathbf{y}_m$ in Y to a new spatial location such that it coincides with a point $\mathbf{x}_n$ in X, i.e., $\mathbf{x}_n = \tau(\mathbf{y}_m)$, and $N_P = \sum_{n,m=1}^{N,M} p^{(i-1)}(\mathbf{y}_m|\mathbf{x}_n) \leq N$.

3.2 *Global Shape Constraint Using Landmark Correspondences*

Given a set of landmarks $\dot{X} \in X$ and $\dot{Y} \in Y$, we have the correspondence between each pair of points $\dot{x}_j \leftrightarrow \dot{y}_j$, where $\dot{x}_j \in \dot{X}$ and $\dot{y}_j \in \dot{Y}$. Hence, our optimal transformation function must minimize the total distance between all pairs of the corresponding $\dot{x}_j$ and $\dot{y}_j$ as follows:

$$E_G = \sum_j \|\dot{x}_j - \dot{y}_j\|^2. \tag{7}$$

To avoid possible singularity in the matrix inverting operation, we revise Eq. (7) as follows:

$$E_G = \sum_{m,n}^{M,N} \mathbf{A}_{m,n}\|\mathbf{x}_n - \tau(\mathbf{y}_m)\|^2, \tag{8}$$

where $\mathbf{A}_{M\times N}$ is landmark coefficient matrix; $\mathbf{A}_{m,n} = 1$ if $(\mathbf{x}_n, \mathbf{y}_m) \in L$, otherwise 0; and L is a set containing all pairs of landmark correspondences.

3.3 *Local Neighborhood Structure Constraint*

To keep points within a neighborhood relatively close after transformation and points far apart distant, SNE[17] is employed. Let r_{ij} be the probability that two points $\mathbf{y}_i$ and $\mathbf{y}_j$ are neighbors before transformation and s_{ij} be the probability that these two points become neighbors after transformation τ. A constraint on local structure is represented as the minimization of the cost function, which is the sum of Kullback–Leibler divergences between r_{ij} and s_{ij} distributions over neighbors of each point:[17]

Downloaded From: https://www.spiedigitallibrary.org/journals/Journal-of-Electronic-Imaging on 23 Apr 2021
Terms of Use: https://www.spiedigitallibrary.org/terms-of-use

$$E_L = \sum_{ij} r_{ij} \log \frac{r_{ij}}{s_{ij}} = \sum_i \mathrm{KL}(\mathbf{R}_i \| \mathbf{S}_i), \tag{9}$$

where

$$r_{ij} = \frac{\exp(-\beta_2 \|\mathbf{y}_i - \mathbf{y}_j\|^2)}{\sum_{k \neq i} \exp(-\beta_2 \|\mathbf{y}_i - \mathbf{y}_k\|^2)} \quad \text{and} \quad s_{ij} = \frac{\exp[-\|\tau(\mathbf{y}_i) - \tau(\mathbf{y}_j)\|^2]}{\sum_{k \neq i} \exp[-\|\tau(\mathbf{y}_i) - \tau(\mathbf{y}_k)\|^2]}.$$

3.4 *Optimization and Algorithm*

We define the transformation function τ, as the initial position $\mathbf{y}_m$, plus a displacement function $\mathbf{f}(\mathbf{y}_m)$, $\tau(\mathbf{y}_m) = \mathbf{y}_m + \mathbf{f}(\mathbf{y}_m)$. We adopt the following transformation function:[6]

$$\mathbf{T} = \tau(\mathbf{Y}, \mathbf{W}) = \mathbf{Y} + \mathbf{G}\mathbf{W}, \tag{10}$$

where $\mathbf{G}_{M\times M}$ is a kernel matrix with elements $g_{ij} = G(\mathbf{y}_i, \mathbf{y}_j) = \exp(-\frac{1}{2}\|\frac{\mathbf{y}_i - \mathbf{y}_j}{\beta}\|^2)$ and $\mathbf{W}_{M\times D} = (\mathbf{w}_1, \ldots, \mathbf{w}_M)^{\mathrm{T}}$ is a coefficients matrix. To maintain topological structure of the point set, we enforce motion coherence, so the transformation model moves neighborhood points coherently:[6,30]

$$E_{\mathrm{MC}} = \mathrm{tr}(\mathbf{W}^{\mathrm{T}}\mathbf{G}\mathbf{W}). \tag{11}$$

The objective function of our method integrates motion coherence, local, and global constraints in Eq. (5) as follows:

$$Q(\boldsymbol{\theta}, \sigma^2) = \frac{1}{2\sigma^2} \sum_{n,m=1}^{N,M} p^{i-1}(\mathbf{y}_m|\mathbf{x}_n)\|\mathbf{x}_n - \tau(\mathbf{y}_m)\|^2 + \frac{N_P D}{2} \ln \sigma^2 + \frac{\lambda_1}{2} E_{\mathrm{MC}} + \frac{\lambda_2}{2} E_L + \frac{\lambda_3}{2} E_G, \tag{12}$$

where λ_1, λ_2, and λ_3 are regularization weights for motion coherence, local structure, and correspondence constraints, respectively.

We obtain the coefficient matrix $\mathbf{W}$ by taking the derivative of Eq. (12) with respect to $\mathbf{W}$ and setting it equal to zero:

$$\begin{aligned}[\mathrm{diag}(\mathbf{P1})\mathbf{G} &+ \sigma^2\lambda_1\mathbf{I} + \sigma^2\lambda_2\mathbf{J}\mathbf{G} + \sigma^2\lambda_3\mathrm{diag}(\mathbf{A1})\mathbf{G}]\mathbf{W} \\ &= [\mathbf{P}\mathbf{X} - \mathrm{diag}(\mathbf{P1})\mathbf{Y} - \sigma^2\lambda_2\mathbf{J}\mathbf{Y} - \sigma^2\lambda_3\mathrm{diag}(\mathbf{A1})\mathbf{Y} + \sigma^2\lambda_3\mathbf{A}\mathbf{X}],\end{aligned} \tag{13}$$

where $\mathbf{1}$ denotes a column vector of all ones, $\mathbf{I}$ is an identity matrix, $\mathrm{diag}(\mathbf{v})$ denotes the diagonal matrix created from the vector $\mathbf{v}$, and

$$\mathbf{J} = [\mathrm{diag}(\mathbf{R1}) - 2\mathbf{R} + \mathrm{diag}(\mathbf{1}^{\mathrm{T}}\mathbf{R})].$$

Similarly, we obtain σ^2 by taking the derivative of Eq. (12) with respect to σ^2 and setting it to zero

$$\sigma^2 = \frac{1}{N_P D}\{\mathrm{tr}[\mathbf{X}^{\mathrm{T}}\mathrm{diag}(\mathbf{P}^{\mathrm{T}}\mathbf{1})] - 2\mathrm{tr}(\mathbf{P}\mathbf{X}^{\mathrm{T}}\mathbf{T}) + \mathrm{tr}[\mathbf{T}^{\mathrm{T}}\mathrm{diag}(\mathbf{P1})\mathbf{T}]\}, \tag{14}$$

where $\mathrm{tr}(\cdot)$ refers to the trace of a matrix and $N_P = \mathbf{1}^{\mathrm{T}}\mathbf{P}\mathbf{1}$. Our algorithm is summarized in Algorithm 1.

Downloaded From: https://www.spiedigitallibrary.org/journals/Journal-of-Electronic-Imaging on 23 Apr 2021
Terms of Use: https://www.spiedigitallibrary.org/terms-of-use

Algorithm 1 The proposed non-rigid point set registration.

Input: Point sets $X = \{x_1, x_2, \ldots, x_N\}$ and $Y = \{y_1, y_2, \ldots, y_M\}$

Output: Correspondence probability, **P**, and the transformed point set **T**

Initialization:

$\sigma^2 \leftarrow \frac{1}{\mathrm{DNM}} \sum_{m,n=1}^{M,N} \|\mathbf{x}_n - \mathbf{y}_m\|^2$,

$\mathbf{W} \leftarrow 0$

Construct: $\mathbf{G}: g_{ij} \leftarrow \exp\left(-\frac{1}{2}\left\|\frac{\mathbf{y}_i - \mathbf{y}_j}{\beta_1}\right\|^2\right)$

while convergence of Q **do**

E-step:

  Compute the posterior probabilities $p(\mathbf{y}_m|\mathbf{x}_n)$ for correspondences following Eq. (6)

M-step:

  Update the weight matrix **W** using Eq. (13)

  Update **T** using Eq. (10)

  Update σ^2 using Eq. (14)

end while

return

4 Results and Discussion

4.1 *Experimental Data and Settings*

In our experiments, we use the publicly available 2D dataset[43] and 3D human pose dataset captured by Microsoft Kinect II.[44] The 2D dataset contains point sets of tools such as scissors, pincer, pliers, and knives. Each tool has five different shapes and each shape contains about 17,000 points. In our 2D tools data experiments, we set the parameters of our method as follows: $\lambda_1 = 8.0$, $\lambda_2 = 1.0$, $\lambda_3 = 120.0$, $\beta_1 = 1.0$, $\beta_2 = 10.0$, and the maximum number of iterations of EM is 50. The 3D human body dataset includes four human subjects with different body shapes and sizes having poses such as standing and squatting. Each point set consists of more than 12,000 points. In our experiments on this dataset, the parameters of our proposed method are as follows: $\lambda_1 = 2.0$, $\lambda_2 = 1.0$, $\lambda_3 = 150.0$, $\beta_1 = 1.0$, $\beta_2 = 15.0$, and the maximum number of iterations of EM is 50. In all our experiments, we manually select five landmarks (except in some experiments, Sec. 4.3, in which we use different numbers of landmarks) in both the tools and human datasets, and hence landmark correspondences are known. Figure 3 shows the different landmarks used in the point sets of both datasets. The tools and human point sets were downsampled by a factor of 7 and 5 in our experiments, respectively. After downsampling, the number of points in the tools case is about 2300, and the number of points in the human case is about 2600. We compute the registration error with a normalized Euclidean distance between the point of the input point set and the corresponding point of the target point set as follows:

$$\varepsilon = \frac{1}{N} \sum_{i,j} \|\mathbf{x}_i - \mathbf{y}_j\|_2, \tag{15}$$

where $\mathbf{x}_i \in \mathbf{X}$, $\mathbf{y}_j \in \mathbf{Y}$ is the estimated corresponding point of $\mathbf{x}_i$ after registration and N is the number of points in point set $\mathbf{X}$. We evaluate our method in the following three aspects: (1) the different degrees of deformation, (2) the different numbers of landmarks, and (3) the impact of incorrect correspondences between landmarks.

Downloaded From: https://www.spiedigitallibrary.org/journals/Journal-of-Electronic-Imaging on 23 Apr 2021
Terms of Use: https://www.spiedigitallibrary.org/terms-of-use

4.2 *Robustness with Respect to the Degree of Deformation*

We evaluate our proposed method with different degrees of deformations and compare with the following state-of-the-art methods: CPD,[6] LSP,[8] and point set registration by preserving global and local structures[11] using both tools and human point sets. We set three degrees of deformations in both the tools and human datasets: small, medium, and large. In tools, for each tool type, we select first and second shapes for small deformation, first and fourth shapes for medium deformation, and first and fifth shapes for large deformation. Similarly, in human cases, we select three combinations of human poses for different degrees of deformations. In particular, we select the both hands-down pose versus three other human poses of raising both hands-up for small, medium, and large deformations [Fig. 2(b)], respectively. In addition, we also select three other combinations of squat poses in the human point sets for three degrees of deformations. We select the both hands-up pose versus three other squat poses: squat starting pose, half squat pose, and full squat pose, see Fig. 1(b) column 1 and 2 for examples of half squat and full squat poses, respectively.

Figure 1 shows different registration results of the tools and human point sets using our method. In this figure, the top two rows show the input and template point sets, respectively. The bottom row shows the registration results of our proposed method. Figure 1(a) shows the point sets and results of the tools point sets, whereas Fig. 1(b) shows point sets and registration results of the human point sets. In each case, the input point sets are of great deformation. The results show very close alignments, which demonstrates the robustness of our proposed method.

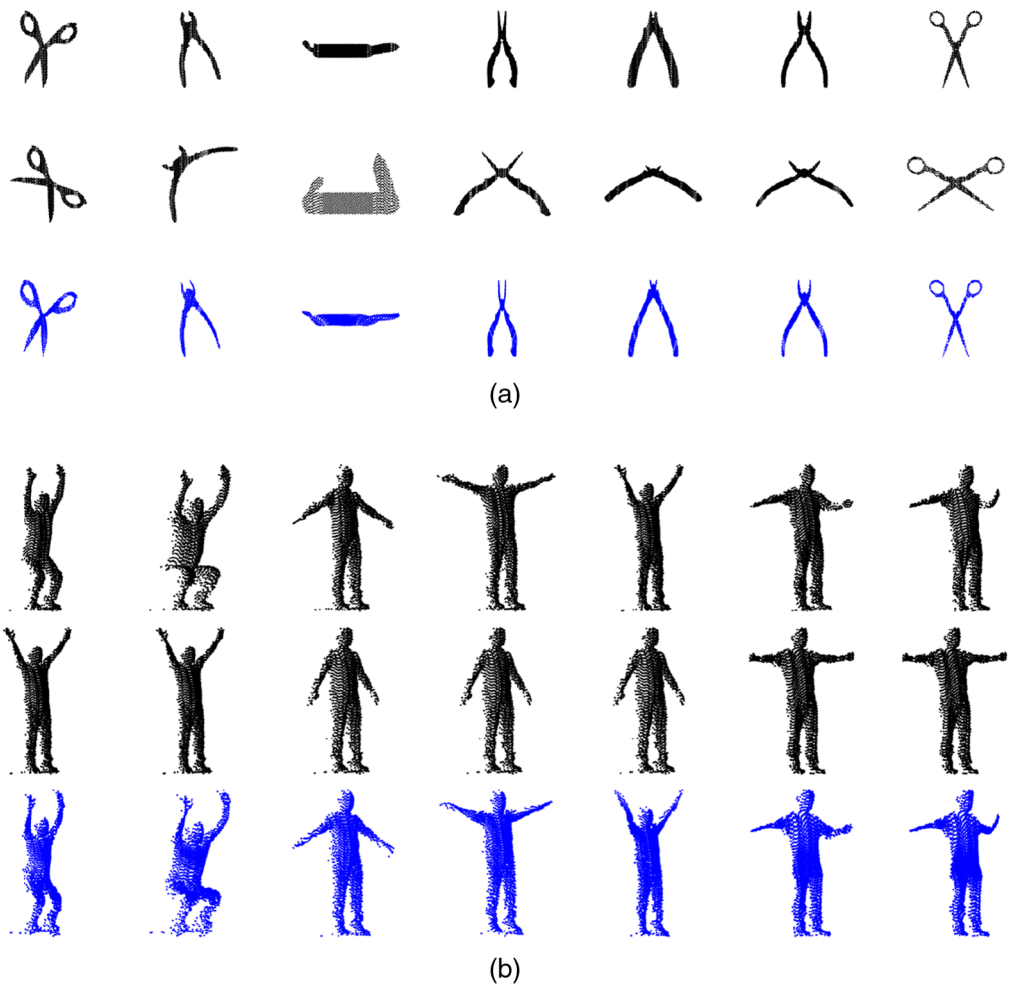

Fig. 1 Exemplar registration results of (a) tools and (b) human point set using our method. Top row shows the input point sets; middle row shows the template point sets; bottom row shows the registration results by which the template is transformed to align with the input in each column.

Downloaded From: https://www.spiedigitallibrary.org/journals/Journal-of-Electronic-Imaging on 23 Apr 2021
Terms of Use: https://www.spiedigitallibrary.org/terms-of-use

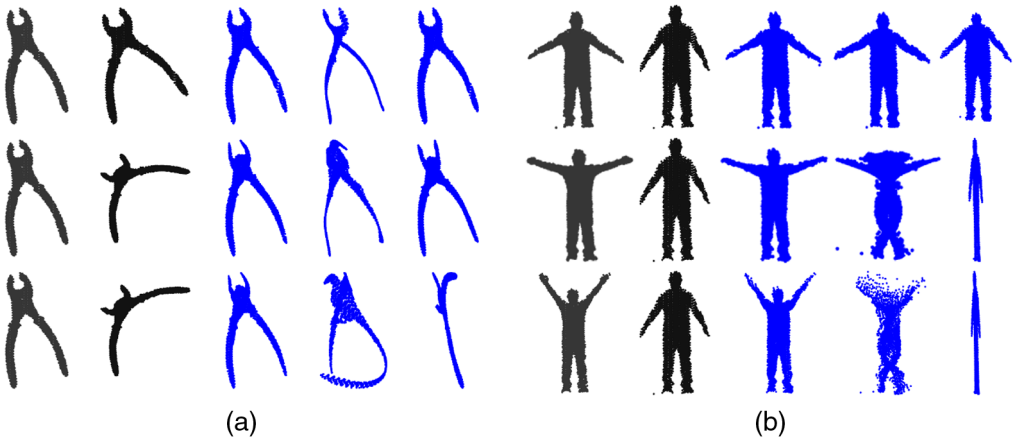

Fig. 2 Exemplar registration results with three degrees of deformation: results of pair of (a) tool point sets and (b) human point sets. The left two columns of each figure are the inputs, and the following three columns are results of our method, CPD, and LSP, respectively.

Figure 2 shows the qualitative registration results of both Fig. 2(a) 2D tools and Fig. 2(b) 3D human body datasets of three degrees of deformation (small, medium, and large) in the top, middle, and bottom rows, respectively. In this figure, the first two columns are input and template point sets, whereas the remaining three columns are the registration results of our method, CPD,[6] and LSP.[8] For the 2D tools dataset, both our method and LSP have better registration results than CPD in a small degree of deformation. In the medium degree of deformation, CPD fails to maintain structure in the upper part of the tool. Our method and LSP exhibit better results than CPD in this case, but the structure of the tip of the tool (upper part) from our method is better than that of LSP. Finally, in the large degree of deformation, our method shows better results than the other two methods; both CPD and LSP completely fail to maintain the shape of the tool. For the 3D human body dataset, our method and CPD generate more accurate results than LSP in a small degree of deformation. In the medium degree of deformation, CPD fails to maintain the shape of the head and has twisted legs, LSP maintains the local structure but is inflexible in this case, and our method generates an accurate result. For a large degree of deformation, both CPD and LSP fail to maintain the human body shape, but our method shows better results (but has some artifacts in the hand regions). In both datasets, our method shows significantly better results by maintaining both local and global structures, especially in a large degree of deformation, which shows the importance of preserving local neighborhood structure and using landmark correspondences.

Tables 1 and 2 list the quantitative registration errors with respect to different degrees of deformation and a comparison with the CPD[6] and LSP[8] methods for the 2D tools and 3D human body datasets. We have three degrees of deformation: small, medium, and large (an example of each case is shown in Fig. 2). For each degree of deformation, the best and the second-best results are highlighted in bold and italic fonts, respectively. Each experiment was repeated five times. Our method exhibits the smallest registration error [and standard deviation (STD)] in

Table 1 Average registration error using the tools dataset with respect to three degrees of deformation.

	Degrees of deformation		
Method	Small	Medium	Large
Our	*2.54 (0.78)*	**3.11 (1.18)**	**3.49 (1.61)**
CPD	4.78 (2.65)	6.13 (2.89)	*7.18 (3.1)*
LSP	**2.33 (0.41)**	*4.71 (3.68)*	12.98 (17.87)

Downloaded From: https://www.spiedigitallibrary.org/journals/Journal-of-Electronic-Imaging on 23 Apr 2021
Terms of Use: https://www.spiedigitallibrary.org/terms-of-use

Table 2 Average registration error using the human body dataset with respect to three degrees of deformation.

Method	Degrees of deformation		
	Small	Medium	Large
Our	*16.03 (4.84)*	**17.21 (6.04)**	**17.47 (5.01)**
CPD	**14.10 (5.71)**	*24.01 (6.91)*	*27.66 (4.78)*
LSP	44.84 (57.29)	174.31 (55.40)	206.36 (17.48)

almost all cases except the cases of small deformations in both 2D and 3D. In these cases, our method's registration error is slightly higher than LSP's registration error by 0.21 in 2D and slightly higher than CPD's registration error by 1.93 in 3D. The average registration errors, by combining both 2D and 3D deformation results for each method, of our method, CPD, and LSP are 9.98, 13.98, and 74.26, respectively. Our method has the lowest average registration error and is 29% better than the second-best result. It is evident that our method has a smaller registration error (STD) than the other methods as the deformation degree increases.

4.3 *Number of Landmarks*

We evaluate our method with different numbers of corresponding landmarks in the point sets to understand the impact of landmarks in registration accuracy. To conduct this experiment, seven landmarks are identified manually in each point set for correspondence. Figure 3 shows a few sample point sets with landmarks marked using green dots.

In each point set, we marked up to seven landmarks that are used to conduct experiments. In this experiment, we select the point sets with large deformations between them (Fig. 4), and the corresponding landmark pairs are fixed. For example in the human body point sets, we have a fixed set of the following seven pairs of corresponding landmarks between two point sets: head, right foot, left foot, right hand, left hand, left elbow, and right elbow, respectively. For each x, we randomly selected x pairs of corresponding landmarks from the fixed set of landmark pairs.

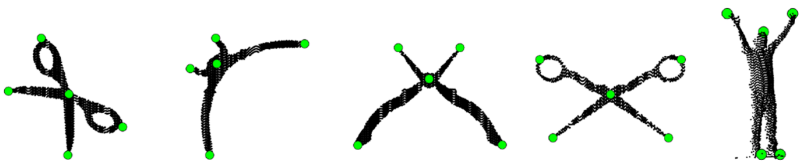

Fig. 3 Examples of landmarks (depicted with green dots) in our point sets.

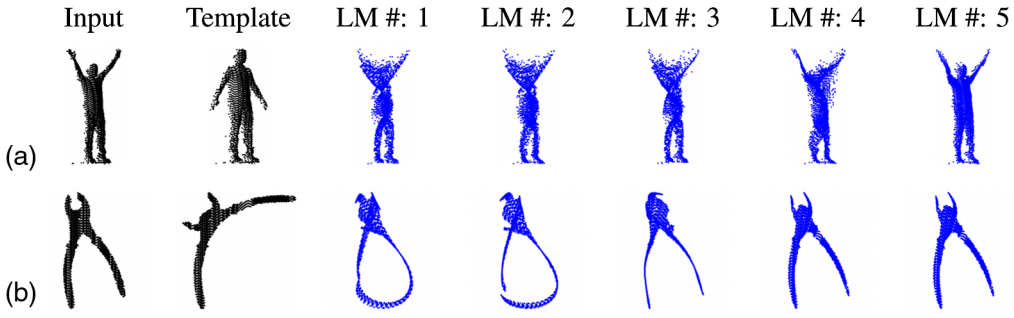

Fig. 4 Registration results of our method using different numbers (up to five) of landmarks. The first two left columns show the input and template point sets, respectively. Columns 3 to 7 show the results using different numbers of landmarks. Row (a) shows the results of the human body dataset, and row (b) shows the results of the tools dataset.

Downloaded From: https://www.spiedigitallibrary.org/journals/Journal-of-Electronic-Imaging on 23 Apr 2021
Terms of Use: https://www.spiedigitallibrary.org/terms-of-use

Figure 4 illustrates the registration results using different numbers (up to five) of landmarks in our method. Figure 4(a) shows the registration results of the human body dataset, and Fig. 4(b) shows the registration results of the tools dataset. The template and input point sets depict large deformations. Each row depicts a case with the left two columns showing the input and the template point sets. The remaining columns in a row show the registration results using an increasing number of landmark pairs from left to right. Figure 4(a) illustrates a challenging case with large and uneven deformations between the input and template point sets. When the number of landmark pairs is <5, the method resulted in poor registration. In human cases, arms and head are fuzzy or "vaporized." As the number of landmark pairs reaches five, the results gain significant improvement due to more precise shape constraints. This trend is also demonstrated in the registration of the tools case as shown in Fig. 4(b), but it shows good registration results even in <5 landmark pairs. In particular, Fig. 4(b) shows improved registration results when the number of landmark pairs is four or more. Therefore, it is fair to say that the minimum number of landmarks needed depends on the degree of disparity between the point sets.

Table 3 presents the average registration errors and standard deviations of our method using a different number of corresponding landmarks for the 2D tools and 3D human body cases. In the case of the 2D tools, we choose two shapes of the scissor tool type with a large degree of deformations between them. In the 3D human case, we choose two poses with a large degree of deformation between the poses of the human datasets. For each number of landmarks used, we repeated the experiment five times. As the number of landmark correspondences increases, the registration accuracy of our method also increases in both cases.

Figure 5 shows the reduction of the average registration errors when one additional pair of corresponding landmarks is used. The curve with triangles depicts the error reduction of tools point sets, and the curve with solid dots depicts the error reduction of human point sets. It is clear that, for the tools point sets, the error reduction becomes very small when four or more landmarks are used. The trend is mostly true for human point sets. However, the error is greatly reduced when six landmarks are used. This is probably due to the complexity of the human point sets, i.e., a large degree of 3D deformation.

Table 3 Average registration error of our method with different numbers of landmarks.

Number of landmarks	Tools	Human
1	4.61 (2.21)	23.2 (1.58)
2	3.13 (1.22)	22.53 (1.98)
3	2.24 (0.03)	20.73 (2.48)
4	2.2 (0.03)	19.27 (3.41)
5	2.19 (0.04)	18.98 (2.99)
6	2.16 (0.03)	16.32 (3.11)
7	2.13 (0.02)	14.67 (2.31)

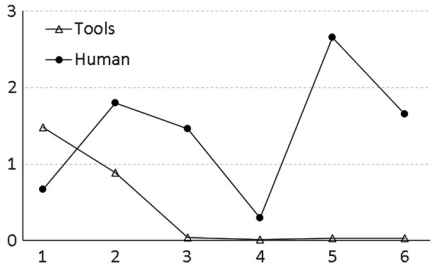

Fig. 5 Error reduction as additional landmarks are included.

Downloaded From: https://www.spiedigitallibrary.org/journals/Journal-of-Electronic-Imaging on 23 Apr 2021
Terms of Use: https://www.spiedigitallibrary.org/terms-of-use

4.4 *Incorrect Landmark Correspondence*

To evaluate the impact of incorrect landmark correspondence, we create three incorrect correspondence cases for each dataset and repeat each registration five times. Figure 6 shows the results of using incorrect correspondences in our registration method. Figure 6(a) shows registration results of the 2D tools point sets, and Fig. 6(b) shows the registration results of the 3D human point sets. The first two columns show the inputs, and the corresponding landmarks are shown in the same color. The third and fourth columns are the registration results of using correct and incorrect landmark correspondences, respectively. The two symmetric halves of the point sets in columns 3 and 4 are colored in green and blue for visual comparison.

For the 2D tools dataset, the registration result [fourth column of Fig. 6(a)] of the first row shows the thin shape of the tool that is twisted in the middle. This is because the left and right landmark correspondences at the top and bottom regions are swapped between input and template point sets. In particular, the left tip landmark (yellow) and right tip landmark (black) of the input point set correspond to the right tip landmark (yellow) and left tip landmark (black) of the template point set. In contrast, the registration result is accurate, and colored points appear in the correct region if correct correspondences are used (third column of Fig. 6). Similar incorrect left and right correspondences between the landmarks at the bottom regions of the tool point set are used. In the second case (middle row), the registration result is similar to the result of the first row, i.e., twisted in the middle part of the tool and thin shape as a result of incorrect landmark correspondences. In the last case (bottom row), not only left and right landmark correspondences at the top regions but also landmark correspondences at the middle and lower right handle regions between input and template point sets are swapped. In this case, the registration result shows an inaccurate shape of the tool with points from different parts of the tool being mixed.

Similarly, for the 3D human body dataset, head region points are fused with the right shoulder and the upper body is twisted in the top row [fourth column of Fig. 6(b)]. In the middle row, the upper body part is twisted and points from the head are mixed with the left shoulder. The last row is highly inaccurate with twisted and fusion of the different parts of the human body.

Table 4 lists the quantitative registration results of using incorrect landmark correspondences in the three different cases. For the 2D tools dataset, all three cases have similar registration errors (and STDs.). For the 3D human body dataset, the first two cases have better results than

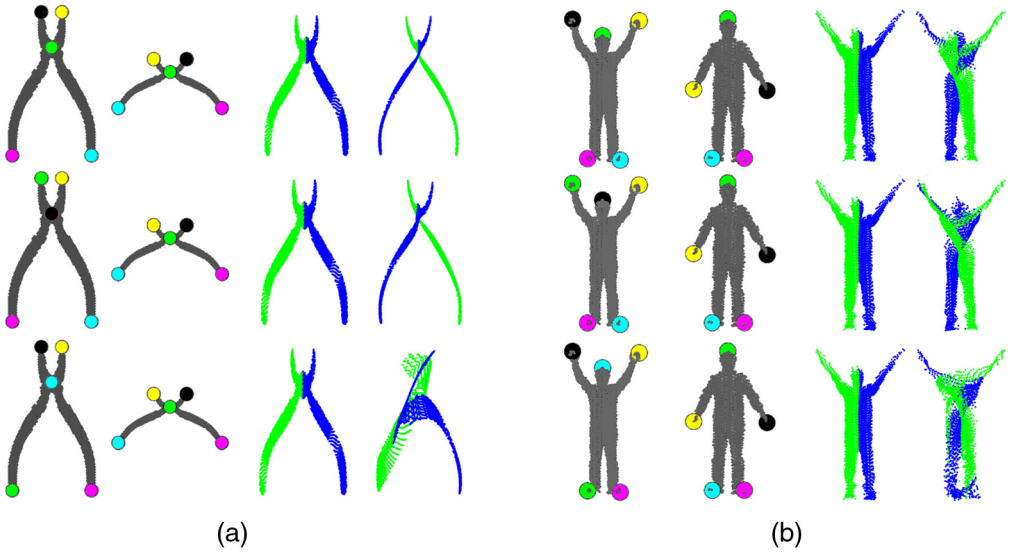

Fig. 6 Exemplar registration results using incorrect landmark correspondences: results of (a) tool point sets and (b) human point sets. The left two columns of each figure are the inputs (and corresponding landmarks have the same color). The third column shows the registration results using correct landmark correspondences, and the last column shows the registration results. For visual comparison, the two symmetric halves of the point sets in columns 3 and 4 are colored in green and blue; only column 3 results show accurate results.

Downloaded From: https://www.spiedigitallibrary.org/journals/Journal-of-Electronic-Imaging on 23 Apr 2021
Terms of Use: https://www.spiedigitallibrary.org/terms-of-use

Table 4 Registration results (STDs.) of our method with different combinations of incorrect landmark correspondences in 2D and 3D datasets.

Incorrect landmark correspondences pair #	Tools	Human
1	6.47 (3.06)	16.63 (0.85)
2	7.06 (2.07)	18.35 (1.89)
3	6.83 (2.06)	24.24 (1.99)

Table 5 Average registration time (in seconds), number of iterations, and average time per iteration (in seconds). The number in parentheses is the standard deviation.

	Time		Number of iterations		Time per iteration	
Method	Tools	Human	Tools	Human	Tools	Human
Our	88.5 (42.3)	117.1 (21.0)	50 (0.0)	50 (0.0)	1.8 (0.8)	2.3 (0.4)
CPD	25.4 (12.1)	40.1 (7.2)	48.3 (3.7)	50 (0.0)	0.5 (0.2)	0.8 (0.1)
LSP	122.2 (65.2)	99.1 (69.5)	47.8 (7.2)	36.2 (15.4)	2.5 (1.2)	2.4 (1.2)

the last case. The average registration errors, when all three cases are combined for each dataset, are 6.78 (2.4) for the 2D tools dataset and 19.74 mm (1.5) for the 3D human body dataset.

4.5 *Time Complexity*

Table 5 lists the average registration time, the average number of iterations of the optimization process, and the average time used per iteration of our method and the state-of-the-art methods. The numbers in the parentheses are the standard derivation. In our experiments, the optimization terminates when it converges or when the maximum number of iterations is reached. The convergence is decided when the objective values between the adjacent two iterations differ by a small fraction, which is 10^{-5}.

Overall, both LSP and our proposed method took more time on average. The average time for CPD is about half of that of the other two methods. This is due to the extra constraints included in the objective functions of LSP and our method. For our method, constraints on local neighborhood structure and global shape using landmark correspondences are included in our optimization process. This timing trend can also be observed in the columns of time per iteration.

The number of iterations for all methods reveals the possible cause of the time complexity. CPD and LSP tend to have an early stop in the optimization process. Such early termination could account for the inferior registration accuracy (refer to Tables 1 and 2 for details). It is likely that the objective function of CPD presents less of a contrast between the global and local optima for the point sets with large deformations, and hence, the optimization process terminates before the maximum number of iteration is reached. Our method consistently ran until the maximum number of iterations was reached. It is expected that further optimization could potentially improve accuracy. On the other hand, a prescribed early stop already achieved superior registration accuracy.

5 Conclusion

This paper proposes a probabilistic non-rigid point set registration method to register point sets with large and uneven deformations. The main idea of our method is to enforce two key constraints: landmark correspondences and preserving local neighborhood structure. Landmarks

Downloaded From: https://www.spiedigitallibrary.org/journals/Journal-of-Electronic-Imaging on 23 Apr 2021
Terms of Use: https://www.spiedigitallibrary.org/terms-of-use

represent the salient points in point sets and can be detected using methods such as scale-invariant feature transform or MeshDOG. The correspondences between landmarks enable us to regulate the optimization process. In addition, by leveraging SNE, we preserve the local structure of the point set by penalizing incoherent transformation within a neighborhood.

We evaluate our method using both 2D tools and 3D human datasets with three different aspects: robustness with respect to the degrees of deformation, number of landmarks in registration, and impact of incorrect landmark correspondences in registration. Our method achieves the smallest average registration errors when both tools and human registration results are combined and compared with other state-of-the-art methods. In particular, quantitative results show that our method is 29% better than the second-best result in deformation experiments. Our results in the medium and large degree of deformations have high qualities than the CPD and LSP. Further analysis of using different numbers of landmarks reveals that a relatively small number of landmarks in our method achieves good registration results. The minimum number of landmarks needed to achieve a satisfactory registration depends on the degree of disparity between the point sets. Our investigation on using incorrect landmark correspondences demonstrates the importance of correct correspondences for accurate registration results. Finally, our study on registration time reports a competitive computational efficiency of the proposed method in comparison with the state-of-the-art methods.

References

1. H. Wang et al., "Multi-perspective terrestrial LiDAR point cloud registration using planar primitives," in *IEEE Int. Geosci. Remote Sens. Symp. (IGARSS)*, pp. 6722–6725 (2016).
2. Q. Lu et al., "Attention-based dense point cloud reconstruction from a single image," *IEEE Access* **7**, 137420–137431 (2019).
3. X. Yuan, D. Feng, and Z. Zuo, *Automatic Construction of Aerial Corridor from Discrete LiDAR Point Cloud*, pp. 449–465. Springer International Publishing (2018).
4. I. Kolesov et al., "A stochastic approach to diffeomorphic point set registration with landmark constraints," *IEEE Trans. Pattern Anal. Mach. Intell.* **38**(2), 238–251 (2016).
5. L. Kong, X. Yuan, and A. M. Maharjan, "A hybrid framework for automatic joint detection of human poses in depth frames," *Pattern Recognit.* **77**, 216–225 (2018).
6. A. Myronenko and X. Song, "Point set registration: coherent point drift," *IEEE Trans. Pattern Anal. Mach. Intell.* **32**, 2262–2275 (2010).
7. S. Ge, G. Fan, and M. Ding, "Non-rigid point set registration with global-local topology preservation," in *IEEE Conf. Comput. Vision and Pattern Recognit. Workshops*, pp. 245–251 (2014).
8. S. Ge and G. Fan, "Non-rigid articulated point set registration with local structure preservation," in *IEEE Conf. Comput. Vision and Pattern Recognit. Workshops*, pp. 126–133 (2015).
9. S. T. Roweis and L. K. Saul, "Nonlinear dimensionality reduction by locally linear embedding," *Science* **290**(5500), 2323–2326 (2000).
10. Y. Zheng and D. Doermann, "Robust point matching for nonrigid shapes by preserving local neighborhood structures," *IEEE Trans. Pattern Anal. Mach. Intell.* **28**(4), 643–649 (2006).
11. J. Ma, J. Zhao, and A. L. Yuille, "Non-rigid point set registration by preserving global and local structures," *IEEE Trans. Image Process.* **25**, 5867–5876 (2016).
12. V. Panaganti and R. Aravind, "Robust nonrigid point set registration using graph-laplacian regularization," in *IEEE Winter Conf. Appl. Comput. Vision*, pp. 1137–1144 (2015).
13. S. Belongie, J. Malik, and J. Puzicha, "Shape matching and object recognition using shape contexts," *IEEE Trans. Pattern Anal. Mach. Intell.* **24**, 509–522 (2002).
14. R. B. Rusu, N. Blodow, and M. Beetz, "Fast point feature histograms (FPFH) for 3D registration," in *IEEE Int. Conf. Rob. Autom.*, pp. 3212–3217 (2009).
15. D. G. Lowe, "Object recognition from local scale-invariant features," in *Proc. Seventh IEEE Int. Conf. Comput. Vision*, Vol. 2, pp. 1150–1157 (1999).
16. A. Zaharescu, E. Boyer, and R. Horaud, "Keypoints and local descriptors of scalar functions on 2D manifolds," *Int. J. Comput. Vision* **100**, 78–98 (2012).

Downloaded From: https://www.spiedigitallibrary.org/journals/Journal-of-Electronic-Imaging on 23 Apr 2021
Terms of Use: https://www.spiedigitallibrary.org/terms-of-use

17. G. E. Hinton and S. T. Roweis, "Stochastic neighbor embedding," in *Advances in Neural Information Processing Systems*, S. Becker, S. Thrun, and K. Obermayer, Eds., Vol. **15**, pp. 857–864, MIT Press (2003).
18. P. J. Besl and N. D. McKay, "A method for registration of 3-D shapes," *IEEE Transa. Pattern Anal. Mach. Intell.* **14**, 239–256 (1992).
19. Y. Chen and G. Medioni, "Object modeling by registration of multiple range images," in *Proc. IEEE Int. Conf. Rob. Autom.*, Vol. 3, pp. 2724–2729 (1991).
20. G. K. L. Tam et al., "Registration of 3D point clouds and meshes: a survey from rigid to nonrigid," *IEEE Trans. Vis. Comput. Graphics* **19**, 1199–1217 (2013).
21. B. Amberg, S. Romdhani, and T. Vetter, "Optimal step nonrigid ICP algorithms for surface registration," in *IEEE Conf. Comput. Vision and Pattern Recognit.*, pp. 1–8 (2007).
22. H. Chui and A. Rangarajan, "A new point matching algorithm for non-rigid registration," *Comput. Vision and Image Understand.* **89**(2), 114–141 (2003).
23. H. Chui and A. Rangarajan, "A new algorithm for non-rigid point matching," in *Proc. IEEE Conf. Comput. Vision and Pattern Recognit., CVPR 2000 (Cat. No.PR00662)*, Vol. 2, pp. 44–51 (2000).
24. S. Gold et al., "New algorithms for 2D and 3D point matching: pose estimation and correspondence," *Pattern Recognit.* **31**(8), 1019–1031 (1998).
25. Y. Tsin and T. Kanade, "A correlation-based approach to robust point set registration," in *Computer Vision—ECCV 2004*, T. Pajdla and J. Matas, Eds., pp. 558–569, Springer Berlin Heidelberg, Berlin, Heidelberg (2004).
26. B. Jian and B. C. Vemuri, "Robust point set registration using Gaussian mixture models," *IEEE Trans. Pattern Anal. Mach. Intell.* **33**(8), 1633–1645 (2011).
27. G. E. Hinton, C. K. I. Williams, and M. D. Revow, "Adaptive elastic models for hand-printed character recognition," in *Advances in Neural Information Processing Systems*, J. E. Moody, S. J. Hanson, and R. P. Lippmann, Eds., Vol. **4**, pp. 512–519, Morgan-Kaufmann (1992).
28. M. Revow, C. K. I. Williams, and G. E. Hinton, "Using generative models for handwritten digit recognition," *IEEE Trans. Pattern Anal. Mach. Intell.* **18**(6), 592–606 (1996).
29. H. Chui and A. Rangarajan, "A feature registration framework using mixture models," in *Proc. IEEE Workshop Math. Methods Biomed. Image Anal., MMBIA-2000 (Cat. No.PR00737)*, pp. 190–197 (2000).
30. A. L. Yuille and N. M. Grzywacz, "The motion coherence theory," in *Proc. Second Int. Conf. Comput. Vision*, pp. 344–353 (1988).
31. G. Wang and Y. Chen, "Fuzzy correspondences guided Gaussian mixture model for point set registration," *Knowl.-Based Syst.* **136**, 200–209 (2017).
32. H. Ling and D. W. Jacobs, "Shape classification using the inner-distance," *IEEE Trans. Pattern Anal. Mach. Intell.* **29**, 286–299 (2007).
33. J. Ma et al., "Robust point matching via vector field consensus," *IEEE Trans. Image Process.* **23**, 1706–1721 (2014).
34. G. Wang et al., "Learning coherent vector fields for robust point matching under manifold regularization," *Neurocomputing* **216**, 393–401 (2016).
35. J. Ma et al., "Nonrigid point set registration with robust transformation learning under manifold regularization," *IEEE Trans. Neural Networks Learn. Syst.* **30**, 3584–3597 (2018).
36. G. Wang, Y. Chen, and X. Zheng, "Gaussian field consensus: a robust nonparametric matching method for outlier rejection," *Pattern Recognit.* **74**, 305–316 (2018).
37. A. Zaharescu et al., "Surface feature detection and description with applications to mesh matching," in *IEEE Conf. Comput. Vision and Pattern Recognit.*, pp. 373–380 (2009).
38. M. Belkin, P. Niyogi, and V. Sindhwani, "Manifold regularization: a geometric framework for learning from labeled and unlabeled examples," *J. Mach. Learn. Res.* **7**, 2399–2434 (2006).
39. G. Wang et al., "Context-aware Gaussian fields for non-rigid point set registration," in *IEEE Conf. Comput. Vision and Pattern Recognit. (CVPR)*, pp. 5811–5819 (2016).
40. Z. Zhang, Y. Dai, and J. Sun, "Deep learning based point cloud registration: an overview," *Virtual Reality Intell. Hardware* **2**(3), 222–246 (2020).
41. Y. Wang and J. M. Solomon, "Deep closest point: learning representations for point cloud registration," in *IEEE Int. Conf. Comput. Vision (ICCV)* (2019).

Downloaded From: https://www.spiedigitallibrary.org/journals/Journal-of-Electronic-Imaging on 23 Apr 2021
Terms of Use: https://www.spiedigitallibrary.org/terms-of-use

42. C. M. Bishop, *Neural Networks for Pattern Recognition*, Oxford University Press, Inc., New York (1995).
43. A. M. Bronstein et al., "Analysis of two-dimensional non-rigid shapes," *Int. J. Comput. Vision* **78**, 67–88 (2008).
44. X. Yuan et al., "Automatic feature point detection and tracking of human actions in time-of-flight videos," *IEEE/CAA J. Autom. Sin.* **4**(4), 677–685 (2017).

Amar Maharjan received his BS degree in computer science and his MS degree in computer science and information technology from the Tribhuvan University, Nepal, in 2005 and 2009, respectively. He is currently a PhD candidate and a member of the Computer Vision and Intelligent Systems Laboratory at the University of North Texas (UNT). He is a recipient of the UNT's Multi-cultural Scholastic Award 2017 and a UNT-I International Education Scholarship 2018–2019. His research interests include computer vision, data mining, and artificial intelligence.

Xiaohui Yuan received his BS degree in electrical engineering from Hefei University of Technology, China, in 1996 and his PhD in computer science from Tulane University in 2004. He is currently an associate professor at the University of North Texas. His research interests include computer vision, artificial intelligence, data mining, and machine learning. His research findings have been published in more than 160 peer-reviewed papers. He is the editor-in-chief of the *International Journal of Smart Sensor Technologies and Applications*, serves on the editorial board of several international journals, and chairs several international conferences. He was a recipient of the Ralph E. Powe Junior Faculty Enhancement Award in 2008.

Qiang Lu received his MS degree and his PhD in computer science and information from Hefei University of Technology. He is an associate professor at the School of Computer and Information of Hefei University of Technology and a member of the Key Laboratory of Knowledge Engineering with Big Data (Hefei University of Technology) of Ministry of Education. His primary research interests include visualization and computer graphics. He is a member of the IEEE and CCF.

Yuqi Fan received his BS and MS degrees in computer science and engineering from Hefei University of Technology in 1999 and 2003, respectively, and his PhD in computer science and engineering from Wright State University in 2009. He is an associate professor at the School of Computer Science and Information Engineering, Hefei University of Technology, China. His research interests include blockchain, computer networks, cloud computing, and cyber-physical systems.

Tian Chen received her PhD at Hefei University of Technology in 2011. She is an associate professor at the School of Computer Science and Information Engineering, Hefei University of Technology, China. Her current research interests include affective computing, artificial intelligence, and designs for testing.

Downloaded From: https://www.spiedigitallibrary.org/journals/Journal-of-Electronic-Imaging on 23 Apr 2021
Terms of Use: https://www.spiedigitallibrary.org/terms-of-use